ppm), but its conversion to **11b** (methyl protons 1.47, 1.73 ppm); methine proton 3.38 ppm) was much faster than for the ammine analogues. This may be related to a slightly smaller steric interaction of the chelating ethylenediamine ligand with the rest of the complex. The isomerization occurred too rapidly to allow a ^{13}C spectrum to be obtained for **9b**, but a spectrum was obtained for **11b**. It showed peaks due to the methyl groups at 25.45 and 30.60 ppm, to the methine carbon at 73.19 ppm, and to carboxyl carbon at 175.59 ppm. There were six peaks in the range 45–53 ppm, four from the four distinct ethylenediamine C atoms of **11b**, one from unreacted Pt(en)(D$_2$O)$_2{}^{2+}$, and one from the quaternary carbon atom of coordinated penicillamine. All of the penicillamine peaks except those from the methyl groups were shifted significantly to lower shielding compared with those of the free ligand.

Conclusions. The conditions of our experiments did not, and were not intended to, mimic those existing in vivo. Our results, however, do show the types of complexes that form between diammineplatinum(II) and thiolate amino acids and derivatives when very labile (aqua) leaving groups bound to platinum provide no kinetic hindrance to coordination of the sulfur donor. When leaving ligands are less labile, as with *cis*-Pt(NH$_3$)$_2$Cl$_2$, reactions such as ammine loss may be competitive with chloride displacement. Relatively complex mixtures of oligomeric complexes with Pt–S–Pt bridges may then be formed rather than simple dinuclear

species. In a living organism, the concentration of platinum complexes will be much less than in our studies, so that, unless dimers are already present before the complexes are injected, formation of compounds with Pt–S–Pt bridges is unlikely. It is, however, possible that thiolate sulfur may form bridges between platinum and another metal present in higher concentration (e.g., Cu^{2+}, Fe^{n+}).

In agreement with the results of others cited earlier, we have found that coordination of thiolate sulfur to platinum always labilizes coordinated ammonia (presumably initially ammonia trans to sulfur). We have shown qualitatively that this labilization is very dependent on the structure of the thiolate ligand, apparently being maximized when the ligand contains other potential donor atoms so located that they can form a five- or six-membered chelate ring.

Contribution from the Departments of Chemistry, The University of Michigan, Ann Arbor, Michigan 48109, and The University of North Carolina, Chapel Hill, North Carolina 27599-3290

Structurally Diverse Manganese(III) Schiff Base Complexes: Chains, Dimers, and Cages

Joseph A. Bonadies,[1] Martin L. Kirk,[2] Myoung Soo Lah,[1] Dimitri P. Kessissoglou,[1,3] William E. Hatfield,*[2] and Vincent L. Pecoraro*[1,4]

Manganese(III) forms a rich variety of complexes with the dianion of the Schiff base ligand *N,N'*-disalicylidene-2-hydroxypropylenediamine (2-OH-SALPN) and its ring-substituted derivatives. Single crystals of [Mn(2-OH-SALPN)OAc]$_n$ (**1**) are isolated when manganese(III) acetate is reacted with 2-OH-SALPN, in DMF. This infinite chain shows an anti–anti configuration for the bridging acetates. When **1** is dissolved in methanol and 1 equiv of NaOH is added, a dinuclear [Mn^{III}$_2$(2-OH-SALPN)$_2$(CH$_3$OH)]·CH$_3$OH complex, **3**, is isolated. X-ray analysis of crystals of the 5-chloro-2-OH-SALPN derivative **4** show this compound to be a monoalkoxy-bridged species with the longest Mn(III)–Mn(III) separation (3.808 Å) yet observed for a discrete single-atom-bridged dimer. If NaOMe is used as a base rather than NaOH, the first example of a totally encapsulated tetrakis(phenolato)–bis(acetato)-caged sodium cation, **5**, is isolated. Two Mn^{III}(2-OH-SALPN) units are linked by this sodium ion, forming a bimetallic, trinuclear cluster. The variable-temperature magnetic behavior of these materials shows that spin exchange between the manganese ions is weak or nonexistent [**1**, $J = -1.72$ cm^{-1} and $g = 1.97$; **4**, $J = -3.55$ cm^{-1} and $g = 1.95$; **5**, follows Curie–Weiss law behavior with no evident spin exchange between Mn(III) ions ($g_\parallel = 2.00$, $g_\perp = 2.05$, $D = -6.13$ cm^{-1})]. X-ray crystallographic parameters: **1**, C$_{19}$H$_{19}$N$_2$O$_5$Mn, mol wt 410.3, orthorhombic crystal system (*Pnma*), $a = 6.528$ (4) Å, $b = 16.827$ (6) Å, $c = 16.754$ (6) Å, $V = 1840$ (1) Å^3, $Z = 4$, 2054 data collected with $0° < 2\theta < 50°$, 1180 data with $I > 3\sigma(I)$, $R = 0.057$, $R_w = 0.057$; **4**, C$_{36}$H$_{34}$N$_4$O$_8$Mn$_2$Cl$_4$, mol wt 900, monoclinic crystal system (*P2$_1$/c*), $a = 10.944$ (2) Å, $b = 23.275$ (5) Å, $c = 16.047$ (2) Å, $\beta = 99.29$ (1)°, $V = 4034$ (1) Å^3, $Z = 4$, 5315 data collected with $0° < 2\theta < 45°$, 3247 data with $I > 2\sigma(I)$, $R = 0.057$, $R_w = 0.045$; **5**, C$_{44}$H$_{55}$N$_4$O$_{18}$Mn$_2$Na, mol wt 1060, triclinic crystal system (*P$\bar{1}$*), $a = 9.434$ (5) Å, $b = 10.436$ (4) Å, $c = 12.758$ (8) Å, $\alpha = 94.42$ (4)°, $\beta = 105.50$ (4)°, $\gamma = 91.50$ (4)°, $V = 1205$ (1) Å^3, $Z = 1$, 3174 data collected with $0° < 2\theta < 45°$, 2445 data with $I > 3\sigma(I)$, $R = 0.068$, $R_w = 0.068$.

Introduction

The coordination chemistry of manganese in the +2, +3, and +4 oxidation states is receiving considerable attention due to the biological importance of these ions. It is now firmly established that at least three enzymes (manganese superoxide dismutase,[5] azide insensitive catalase,[6] and the photosynthetic oxygen-evolving

complex[7]) use manganese in redox roles at their catalytic center to facilitate the metabolism of the O$_2{}^{r-}$ unit. All three enzymes probably contain Mn(III) in at least one of their catalytic forms. Therefore, an important area of investigation of the bioinorganic chemistry of manganese is the study of the structure and reactivity of Mn(III) complexes composed of biologically relevant heteroatom donor ligands.

An attractive system for modeling the structure and reactivity of these manganoenzymes is dinuclear Mn(III) complexes containing polydentate Schiff base ligands. Both photochemical water oxidation to generate dioxygen[8] and acid-promoted hydrogen peroxide production[9] have been reported for such dimers. To

(1) The University of Michigan.
(2) The University of North Carolina.
(3) Permanent address: Department of Inorganic and General Chemistry, The Aristotelian University of Thessaloniki, Thessaloniki, Greece.
(4) G. D. Searle Biomedical Research Scholar (1986–1989), Alfred P. Sloan Fellow (1989–1991).
(5) Ludwig, M. L.; Pattridge, K. A.; Stallings, W. C. *Manganese in Metabolism and Enzyme Function*; Academic Press: New York, 1986; Chapter 21, p 405.
(6) Beyer, W. F., Jr.; Fridovich, I. *Manganese in Metabolism and Enzyme Function*; Academic Press: New York, 1986; Chapter 12, p 193.

(7) (a) Pecoraro, V. L. *Photochem. Photobiol.* **1986**, *48*, 249. (b) Asmez, J. *Biochim. Biophys. Acta* **1983**, *726*, 1.
(8) Ashmawy, F. M.; McAuliffe, C. A.; Parish, R. V.; Tames, J. *J. Chem. Soc., Dalton Trans.* **1985**, 1391.

understand more fully the chemistry involved in these reactions, we have initiated studies of the solid-state solution behavior of Mn(III)-containing polydentate Schiff base complexes.

In this contribution we present three distinct structural types for manganese(III)–2-OH-SALPN complexes and examine their magnetic behavior. We have observed an infinite chain of Mn^{III}(2-OH-SALPN) units bridged by acetate moieties, a unique monoalkoxy-bridged Mn(III) dimer, and a Mn(III)–Na(I)–Mn(III) structure that encapsulates the central alkali-metal cation by using phenolate and acetate bridges. In the following paper we describe the solution behavior that relates these interesting structures.

Experimental Section

Materials. Salicylaldehyde (SAL) and 1,3-diamino-2-hydroxypropane were obtained from Aldrich Chemical Co. $Mn(CH_3COO)_3 \cdot 2H_2O$ and $Mn(CH_3COO)_2 \cdot 2H_2O$ were obtained from Fluka Co. 5-Chlorosalicylaldehyde (5-Cl-SAL) was obtained from Pfaltz and Bauer. All other chemicals and solvents were reagent grade.

Synthesis. [Mn(2-OH-SALPN)(OAc)]$_n$ (1). A 20-mmol (2.16-mL) amount of salicylaldehyde and 10 mmol (0.9 g) of 1,3-diamino-2-hydroxypropane were reacted under reflux for 1 h in 50 mL of DMF. Then 30 mmol (1.2 g) of NaOH and 10 mmol (2.68 g) of Mn(acetate)$_3 \cdot 2H_2O$ were added with stirring and the reaction mixture was refluxed for 2 h. The deep green-brown solution was cooled to room temperature and filtered, and a white solid was removed (sodium acetate). The dark green-brown filtrate was reduced to one-fifth its initial volume and put into the freezer. A green microcrystalline product was deposited, collected by suction filtration, and dried under vacuum. Single crystals for X-ray analysis were obtained by slow evaporation of the mother reaction solution. Anal. Calcd for $C_{19}H_{19}N_2O_5Mn$ (mol wt 410): C, 55.60; H, 4.63; N, 6.83; Mn, 13.41. Found: C, 55.69; H, 4.57; N, 6.65; Mn, 13.21.

Mn(2-OH-SALPN)(NCS) (2). A 20-mmol (2.16-mL) amount of salicylaldehyde and 10 mmol (0.9 g) of 1,3-diamino-2-hydroxypropane were reacted in 100 mL of methanol under reflux for 1 h. Then 30 mmol (1.2 g) of NaOH and 10 mmol (2.45 g) of Mn(acetate)$_2 \cdot 4H_2O$ were added under N_2 and with stirring. A yellow solid, which proved to be insoluble in all organic solvents and in water, precipitated immediately. This yellow mixture was exposed to air and began to change color from yellow to green, finally giving a deep green solution. Into this solution was added an excess of NH_4SCN, about 0.1 mmol, and the solution concentrated. A green crystalline product was deposited, collected by filtration, and dried under vacuum. The yield of the reaction was 85%. Anal. Calcd for $C_{18}H_{23}N_3O_5SMn$ (mol wt 445): C, 48.54; H, 4.49; N, 9.43; Mn, 12.36. Found: C, 48.81; H, 4.40; N, 9.52; Mn, 12.23.

[Mn$_2$(2-OH-SALPN)$_2$(CH$_3$OH)]·CH$_3$OH (3) and [Mn$_2$(2-OH[5-Cl-SAL]PN)$_2$(CH$_3$OH)]·CH$_3$OH (4). A 20-mmol (2.16-mL) amount of salicylaldehyde and 10 mmol (0.9 g) of 1,3-diamino-2-hydroxypropane were reacted in 100 mL of methanol under reflux for 1 h. Then 20 mmol (0.8 g) of NaOH and 10 mmol (1.98 g) of MnCl$_2$ were added. After it was stirred for 2 h with vigorous aeration, the solution was allowed to slowly evaporate. A green-brown crystalline product was deposited, collected by filtration, and dried under vacuum. The preparation of **4** was identical with that of **3** with the substitution of 5-chlorosalicylaldehyde. X-ray quality crystals formed when the reaction was run at a 20% dilution and the solution was left to slowly evaporate. Anal. Calcd for **3**, $C_{36}H_{38}N_4O_8Mn_2$ (mol wt 764): C, 56.55; H, 4.97; N, 7.33; Mn, 14.40. Found: C, 55.55; H, 4.93; N, 7.55; Mn, 15.13. Calcd for **4** $C_{36}H_{34}N_4O_8Cl_4Mn_2$ (mol wt 900): C, 48.00; H, 3.78; N, 6.22; Cl, 15.56; Mn, 12.22. Found: C, 45.97; H, 3.42; N, 6.13; Cl, 15.52; Mn, 12.75.

[C$_2$H$_9$O$_2$][NaMn$_2$(2-OH-SALPN)$_2$(OAc)$_4$]·2H$_2$O (5). A 20-mmol (2.16-mL) amount of salicylaldehyde and 10 mmol (0.9 g) of 1,3-diamino-2-hydroxypropane were reacted under reflux in 100 mL of methanol for 1 h. Then 20 mmol (0.8 g) of NaOH and 5 mmol (0.27 g) of NaOCH$_3$ were added and allowed to dissolve. A 30-mmol (3.68-g) amount of manganese(II) acetate was added, producing a yellow precipitate. Vigorous aeration and stirring of the solution for approximately $^1/_2$ h redissolved the solid and produced a green solution. This solution was then allowed to evaporate slowly, producing X-ray-quality crystals of **5**. Anal. Calcd for $C_{44}H_{55}N_4O_{18}Mn_2Na$ (mol wt 1060): C, 49.81; H, 5.19; N, 5.28; Mn, 10.38; Na, 2.17. Found: C, 49.16; H, 5.55; N, 5.28; Mn, 10.18; Na, 2.23.

Methods. Infrared spectra were obtained on a Nicolet 60-SX FT-IR instrument as KBr pellets. Chemical analyses were performed by either Galbraith Laboratories, Inc., Knoxville, TN, or Oneida Research Serv-

Table I. Summary of Crystal Data for [Mn(2-OH-SALPN)OAc]$_n$ (1), [Mn$_2$(2-OH[5-Cl-SAL]PN)$_2$(CH$_3$OH)]·CH$_3$OH (4), and [C$_2$H$_9$O$_2$][NaMn$_2$(2-OH-SALPN)$_2$(OAc)$_4$]·2H$_2$O (5)

	1	4	5
formula	$C_{19}H_{19}N_2O_5Mn$	$C_{36}H_{34}N_4O_8-$ Cl_4Mn_2	$C_{44}H_{55}N_4O_{18}-$ Mn_2Na
mol wt	410.3	900.0	1062.8
space group	$Pnma$	$P2_1/c$	$P\bar{1}$
a, Å	6.520 (2)	10.944 (2)	9.434 (5)
b, Å	16.809 (6)	23.275 (5)	10.436 (4)
c, Å	16.729 (6)	16.046 (2)	12.758 (8)
α, deg			94.42 (4)
β, deg		99.29 (1)	105.50 (4)
γ, deg			91.50 (4)
V, Å^3	1833 (1)	4034 (1)	1205 (1)
Z	4	4	1
d_{calc}, g/mL	1.486	1.539	1.464
d_{meas}, g/mL	1.48^a	1.56^b	1.43^b
cryst dimens, mm	0.097 × 0.276 × 0.471	0.47 × 0.16 × 0.30	0.22 × 0.27 × 0.49
radiation	Mo Kα	Mo Kα	Mo Kα
abs coeff, cm^{-1}	6.91	8.78	5.60
scan range, deg	−0.8 to +0.9	−0.8 to +0.9	−0.8 to +0.9
bkgd time ratio	0.8	0.8	0.8
2θ, deg	50	45	45
no. of data collected	1680	5315	3174
no. of data >3$\sigma(I)$	1277		2445
no. of data >2$\sigma(I)$		3247	
final R_1	0.053	0.057	0.068
final R_2	0.055	0.045	0.068
largest residual, e/Å^3	0.25	0.59	0.86

^{a} Hexane/CCl$_4$ flotation. ^{b} Toluene/CCl$_4$ flotation.

ices, Inc., of White Plains, NY. Magnetic susceptibility data were collected with the use of a Foner-type Princeton Applied Research Model 155 vibrating-sample magnetometer. The magnetometer was calibrated with mercury tetrakis(thiocyanato)cobaltate(II).[10] The temperature was measured with a gallium arsenide diode, which has been standardized against a calibrated diode. Diamagnetic corrections for the constituent atoms were made by using Pascal's constants.[11,12] Samples containing approximately 150 mg of finely powdered compound were contained in precision-milled Lucite sample holders. The magnetic susceptibility was measured in a field of 10 kOe. A simplex[13] nonlinear least-squares fitting procedure was used in the analysis of the experimental magnetic susceptibility data. The best fit criterion was the minimum of the function $F = \sum (\chi_i^{obsd} - \chi_i^{calcd})^2 / (\chi_i^{obsd})^2$.

Collection and Reduction of X-ray Data. Single crystals of **1** were grown from a dimethylformamide solution, and single crystals of **4** and **5** were grown from methanol solution. Each crystal was then mounted in a glass capillary, and data were collected on a Syntex P2$_1$ diffractometer. Intensity data were obtained with use of Mo Kα radiation (0.7107 Å) monochromatized from a graphite crystal whose diffraction vector was parallel to the diffraction vector of the sample. Three standard reflections were measured every 50 reflections. Lattice parameters were determined from a least-squares refinement of 15 reflection settings obtained from an automatic centering routine. Table I contains a summary of data collection conditions and results for each structure. The data were reduced by using the SHELX76 program package, and the structure was solved by using MULTAN for **1** and SHELX86 for **4** and **5**.[14] In the subsequent refinement, the function $\sum w(|F_o| - |F_c|)^2$ was minimized, where $|F_o|$ and $|F_c|$ are the observed and calculated structure factor amplitudes. The agreement indices $R_1 = \sum ||F_o| - |F_c||/|F_o|$ and $R_2 = [\sum w(|F_o| - |F_c|)^2/\sum w|F_o|^2]^{1/2}$ were used to evaluate the results. Atomic scattering factors are from ref 15. Hydrogen atoms were located, but

(9) Boucher, L. J.; Coe, C. G. *Inorg. Chem.* **1975**, *14*, 1289.

(10) Brown, D. B.; Crawford, V. H.; Hall, J. W.; Hatfield, W. E. *J. Phys. Chem.* **1977**, *81*, 1303.

(11) (a) Figgis, B. N.; Lewis, J. In *Modern Coordination Chemistry*; Lewis, J., Wilkins, R. G., Eds.; Interscience: New York, 1960; Chapter 6, p 403. (b) Konig, E. *Magnetic Properties of Transition Metal Compounds*; Springer-Verlag: West Berlin, 1966.

(12) Weller, R. R.; Hatfield, W. E. *J. Chem. Educ.* **1979**, *56*, 652.

(13) (a) Soendley, W.; Hext, G. R.; Himsworth, F. R. *Technometrics* **1962**, *4*, 441. (b) Nelder, J. A.; Mead, R. *Comput. J.* **1965**, *7*, 308.

(14) Computations were carried out on an Amdahl 5860 computer. Computer programs used during the structural analysis were from the SHELX program package by George Sheldrick, Institut für Anorganische Chemie der Universität Göttingen, Göttingen, Federal Republic of Germany. Other programs used included ORTEP, a thermal ellipsoidal drawing program by C. K. Johnson, and the direct-methods program MULTAN78 by Peter Main.

Table II. Fractional Atomic Coordinates and Isotropic Thermal Parameters for Non-Hydrogen Atoms of Complex **1**

atom	x	y	z	U, Å^2
Mn1	0.8746 (2)	0.2500 (0)	0.5249 (1)	0.029
O1	0.8758 (6)	0.3258 (2)	0.6072 (2)	0.049
C1	0.8045 (8)	0.3986 (3)	0.6078 (4)	0.048
C2	0.7542 (11)	0.4339 (5)	0.6822 (4)	0.080
C3	0.6841 (13)	0.5104 (6)	0.6850 (6)	0.099
C4	0.6633 (11)	0.5559 (5)	0.6175 (8)	0.101
C5	0.7120 (10)	0.5246 (4)	0.5447 (5)	0.070
C6	0.7793 (8)	0.4440 (3)	0.5380 (4)	0.050
C7	0.8191 (8)	0.4130 (3)	0.4602 (3)	0.046
N1	0.8597 (7)	0.3402 (2)	0.4426 (2)	0.039
C8	0.9000 (10)	0.3238 (4)	0.3575 (3)	0.056
C9	0.7926 (13)	0.2500 (0)	0.3270 (5)	0.047
O2	0.5839 (8)	0.2500 (0)	0.3392 (3)	0.055
O3	0.5351 (7)	0.2500 (0)	0.5021 (3)	0.045
O4	0.2003 (8)	0.2500 (0)	0.4992 (3)	0.047
C10	0.3619 (11)	0.2500 (0)	0.5361 (4)	0.036
C11	0.3598 (13)	0.2500 (0)	0.6257 (6)	0.074
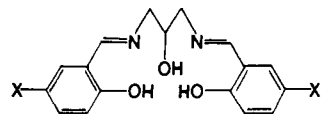
Figure 1. Ligands used in this study: X = H, 2-OH-SALPN; X = Cl, 2-OH-(5-Cl-SAL)PN.
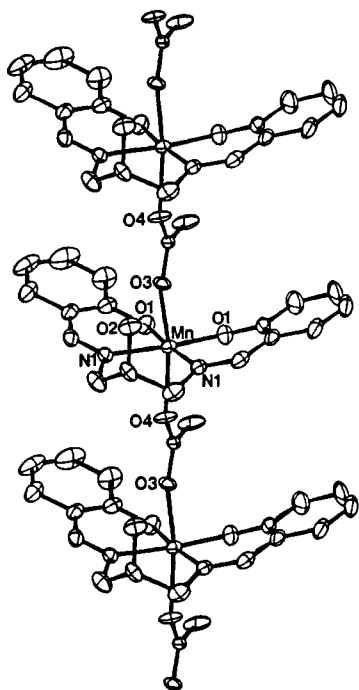
Figure 2. ORTEP diagram of [Mn(2-OH-SALPN)(OAc)]$_n$ (**1**) (showing atom-numbering scheme) with thermal ellipsoids of 50% probability. Multiple units are shown in the figure to illustrate the polymeric nature of the molecule.

not refined, and placed at fixed distances of 0.95 Å from bonded carbon atoms in the final least-squares refinement. All hydrogen atoms were given fixed U values (isotropic temperature factors) of 0.05 Å^2. Fractional atomic coordinates for all non-hydrogen atoms of **1**, **4**, and **5** are shown in Tables II–IV respectively. Tables V–VII list selected bond distances and angles for **1**, **4**, and **5**, respectively. Unique data and final R indices are reported in Table I.

Results and Discussion

Manganese complexes of the dianion of the ligand N,N'-di-salicylidene-2-hydroxypropylenediamine (2-OH-SALPN) and its derivatives, which are shown in Figure 1, have been synthesized

(15) *International Tables for X-Ray Crystallography*; Ibers, J. A., Hamilton, W. C., Eds.; Kynoch Press: Birmingham, England, 1974; Vol. IV, Table 2.2 and 2.3.1.

Table III. Fractional Atomic Coordinates and Isotropic Thermal Parameters for Non-Hydrogen Atoms of Complex **4**

atom	x	y	z	U, Å^2
Mn1	0.1772 (1)	0.3492 (0)	0.5870 (1)	0.043
Mn2	0.0366 (1)	0.2505 (0)	0.4076 (1)	0.037
Cl1	0.6001 (2)	0.3350 (1)	0.9942 (1)	0.083
Cl2	−0.2958 (3)	−0.0157 (1)	0.4308 (2)	0.117
Cl3	−0.0194 (2)	0.5030 (1)	0.2029 (1)	0.090
Cl4	−0.5350 (2)	0.3695 (1)	0.2036 (1)	0.091
O1	0.2423 (5)	0.3967 (2)	0.6952 (3)	0.068
O2	0.1740 (4)	0.2880 (2)	0.4728 (2)	0.039
O3	−0.0785 (4)	0.2009 (2)	0.3433 (2)	0.039
O4	0.2405 (4)	0.4047 (2)	0.5192 (3)	0.055
O5	0.0933 (4)	0.2963 (2)	0.6459 (2)	0.046
O6	−0.0220 (4)	0.3162 (2)	0.3456 (2)	0.041
O7	0.1625 (4)	0.2404 (2)	0.3042 (2)	0.044
N1	0.3443 (5)	0.3064 (2)	0.6142 (3)	0.038
N2	0.1014 (5)	0.1841 (2)	0.4801 (3)	0.039
N3	0.0110 (5)	0.3844 (2)	0.5580 (3)	0.038
N4	−0.1116 (5)	0.2745 (2)	0.4873 (3)	0.038
C1	0.3196 (7)	0.3808 (4)	0.7617 (5)	0.056
C2	0.3284 (8)	0.4114 (4)	0.8390 (6)	0.081
C3	0.4128 (9)	0.3971 (4)	0.9080 (5)	0.072
C4	0.4916 (7)	0.3511 (4)	0.9049 (5)	0.058
C5	0.4893 (7)	0.3208 (3)	0.8337 (4)	0.049
C6	0.4048 (7)	0.3343 (3)	0.7610 (4)	0.043
C7	0.4161 (7)	0.3038 (3)	0.6854 (4)	0.042
C8	0.3827 (7)	0.2764 (4)	0.5434 (4)	0.052
C9	0.2712 (6)	0.2464 (3)	0.4916 (4)	0.046
C10	0.2207 (7)	0.1967 (3)	0.5343 (4)	0.048
C11	0.0468 (7)	0.1356 (3)	0.4866 (4)	0.049
C12	−0.0679 (7)	0.1191 (3)	0.4353 (4)	0.043
C13	−0.1228 (9)	0.0675 (4)	0.4551 (5)	0.058
C14	−0.2270 (9)	0.0478 (3)	0.4062 (6)	0.063
C15	−0.2790 (8)	0.0782 (4)	0.3352 (6)	0.056
C16	−0.2277 (7)	0.1285 (4)	0.3147 (5)	0.047
C17	−0.1228 (6)	0.1519 (3)	0.3649 (4)	0.038
C18	0.1760 (7)	0.4260 (3)	0.4487 (5)	0.048
C19	0.2410 (8)	0.4418 (4)	0.3841 (6)	0.064
C20	0.1836 (9)	0.4645 (4)	0.3090 (6)	0.075
C21	0.0574 (9)	0.4748 (3)	0.2981 (5)	0.064
C22	−0.0095 (8)	0.4606 (3)	0.3591 (5)	0.049
C23	0.0481 (7)	0.4353 (3)	0.4350 (4)	0.043
C24	−0.0274 (7)	0.4174 (3)	0.4957 (4)	0.044
C25	−0.0697 (7)	0.3652 (4)	0.6183 (4)	0.050
C26	−0.0377 (7)	0.3031 (4)	0.6383 (4)	0.051
C27	−0.1087 (7)	0.2602 (4)	0.5763 (4)	0.048
C28	−0.2150 (7)	0.2935 (3)	0.4481 (4)	0.043
C29	−0.2349 (7)	0.3156 (3)	0.3616 (4)	0.040
C30	−0.3579 (7)	0.3290 (3)	0.3258 (5)	0.054
C31	−0.3818 (7)	0.3527 (4)	0.2482 (5)	0.057
C32	−0.2877 (9)	0.3664 (4)	0.2032 (5)	0.061
C33	−0.1678 (8)	0.3536 (3)	0.2366 (4)	0.047
C34	−0.1374 (6)	0.3269 (3)	0.3157 (4)	0.037
C35	0.2242 (9)	0.2920 (4)	0.2864 (5)	0.070
O1M	0.6741 (10)	0.0075 (4)	0.9014 (6)	0.165
C1M	0.6064 (20)	0.0078 (7)	0.8277 (13)	0.194
O2M	0.6274 (11)	0.0960 (5)	0.0013 (6)	0.182
C2M	0.5781 (18)	0.0830 (8)	0.0656 (13)	0.167

as monomeric, dimeric, polymeric, and mixed-metal cage complexes. The general physical properties of these complexes are shown in Table VIII. A detailed discussion of their solution behavior is presented in the following paper.

[Mn(2-OH-SALPN)OAc]$_n$. The reaction of 2-OH-SALPN with 3 equiv of base and 1 equiv of Mn(OAc)$_3$·4H$_2$O produced X-ray-quality crystals of the polymeric manganese acetate chain illustrated in Figure 2. Each manganese(III) in the chain has an equatorial plane composed of the two phenolate oxygen atoms and two imine nitrogen atoms of the ligand. The manganese atoms also lie on a mirror plane along with the central backbone carbon and hydroxyl group, and the axial acetates. The alcohol oxygen on the ligand backbone is protonated and uncoordinated. The acetate bridges are in an anti–anti orientation as previously reported for [Mn(SALEN)OAc]$_n$.[16] The chain axis has unsym-

(16) Davies, J. *J. Chem. Soc., Dalton Trans.* **1973**, 2523.

Table IV. Fractional Atomic Coordinates and Isotropic Thermal Parameters for Non-Hydrogen Atoms of Complex **5**

atom	x	y	z	U, Å^2
Mn1	−0.1118 (1)	0.2041 (1)	0.1681 (1)	0.035
Na1	0.0 (0)	0.0 (0)	0.0 (0)	0.043
O1	−0.0758 (6)	0.0260 (5)	0.1660 (4)	0.049
O2	0.0144 (6)	0.2166 (4)	0.0741 (4)	0.043
O3	−0.3125 (6)	0.1897 (5)	0.0427 (4)	0.047
O4	−0.2460 (6)	0.0514 (6)	−0.0758 (5)	0.058
O5	0.0942 (7)	0.2355 (6)	0.3099 (5)	0.054
O7	−0.1653 (11)	0.4339 (8)	0.3947 (6)	0.101
N1	−0.2340 (7)	0.1830 (6)	0.2755 (5)	0.045
N2	−0.1267 (7)	0.4002 (6)	0.1757 (5)	0.039
C1	−0.0616 (9)	−0.0469 (7)	0.2475 (6)	0.043
C2	0.0202 (11)	−0.1554 (7)	0.2481 (7)	0.057
C3	0.0330 (12)	−0.2360 (8)	0.3324 (8)	0.064
C4	−0.0359 (13)	−0.2125 (9)	0.4149 (8)	0.074
C5	−0.1176 (12)	−0.1057 (9)	0.4140 (7)	0.067
C6	−0.1328 (10)	−0.0210 (7)	0.3312 (6)	0.048
C7	−0.2196 (10)	0.0868 (8)	0.3356 (7)	0.054
C8	−0.3455 (10)	0.2738 (8)	0.2859 (8)	0.067
C9	−0.2856 (12)	0.4147 (9)	0.3046 (9)	0.073
C10	−0.2518 (9)	0.4599 (7)	0.2036 (8)	0.055
C11	−0.0297 (9)	0.4733 (7)	0.1526 (6)	0.042
C12	0.0972 (8)	0.4385 (7)	0.1185 (6)	0.039
C13	0.2039 (9)	0.5336 (7)	0.1170 (7)	0.048
C14	0.3261 (10)	0.5038 (8)	0.0825 (7)	0.056
C15	0.3438 (10)	0.3771 (8)	0.0464 (7)	0.057
C16	0.2393 (9)	0.2824 (7)	0.0433 (7)	0.048
C17	0.1143 (8)	0.3084 (6)	0.0796 (6)	0.034
C18	−0.3418 (9)	0.1165 (7)	−0.0456 (6)	0.043
C19	−0.4954 (11)	0.1060 (9)	−0.1158 (8)	0.064
O1W	0.3100 (12)	0.0834 (11)	0.2789 (9)	0.103
O6	0.0853 (22)	0.4323 (14)	0.4074 (10)	0.069
O6'	0.2055 (34)	0.4660 (15)	0.4072 (14)	0.096
C20	0.1640 (23)	0.3440 (20)	0.3686 (15)	0.163
C21	0.3422 (21)	0.4110 (35)	0.4003 (18)	0.291
O8	0.5664 (54)	0.0522 (34)	0.5780 (33)	0.451
C22	0.5632 (34)	0.1903 (56)	0.5942 (32)	0.391

Table V. Selected Bond Distances (Å) and Angles (deg) for **1**

Mn1–O1	1.876 (3)	Mn1–N1	2.050 (4)
Mn1–O3	2.246 (5)	Mn1–O4	2.167 (5)
O1–Mn1–N1	89.5 (2)	O1–Mn1–O3	97.4 (2)
N1–Mn1–O3	80.8 (1)	O1–Mn1–O4	98.1 (2)
N1–Mn1–O4	85.0 (2)	O3–Mn1–O4	158.8 (2)

Table VI. Selected Bond Distances (Å) and Angles (deg) for **4**

Mn1–O1	2.084 (5)	Mn1–O2	2.317 (4)
Mn1–O4	1.891 (5)	Mn1–O5	1.879 (5)
Mn1–N1	2.067 (5)	Mn1–N3	1.980 (5)
Mn2–O2	1.900 (4)	Mn2–O3	1.887 (4)
Mn2–O6	1.880 (4)	Mn2–O7	2.334 (4)
Mn2–N2	1.994 (4)	Mn2–N4	2.291 (5)
	Mn1–Mn2	3.808 (1)	
O1–Mn1–O2	160.8 (2)	O1–Mn1–O4	90.5 (2)
O1–Mn1–O5	93.3 (2)	O1–Mn1–N1	84.7 (2)
O1–Mn1–N3	98.8 (2)	O2–Mn1–O4	85.7 (2)
O2–Mn1–O5	92.8 (2)	O2–Mn1–N1	76.7 (2)
O2–Mn1–N3	99.9 (2)	O4–Mn1–O5	172.3 (2)
O4–Mn1–N1	93.3 (2)	O4–Mn1–N3	89.5 (2)
O5–Mn1–N1	93.7 (2)	O5–Mn1–N3	83.4 (2)
N1–Mn1–N3	175.5 (2)	Mn1–O2–Mn2	128.9 (2)
O2–Mn2–O3	168.8 (2)	O2–Mn2–O6	95.2 (2)
O2–Mn2–O7	86.1 (2)	O2–Mn2–N2	81.9 (2)
O2–Mn2–N4	98.6 (2)	O3–Mn2–O6	93.8 (2)
O3–Mn2–O7	88.2 (2)	O3–Mn2–N2	89.3 (2)
O3–Mn2–N4	89.1 (2)	O6–Mn2–O7	84.0 (2)
O6–Mn2–N2	176.3 (2)	O6–Mn2–N4	83.4 (2)
O7–Mn2–N2	98.1 (2)	O7–Mn2–N4	166.9 (2)
N2–Mn2–N4	94.7 (2)		

metric Mn–O distances with the Mn–O3 bond being significantly longer (2.246 Å) than Mn–O4 (2.167 Å). The Mn–O and Mn–N bond lengths (Table IV) for equatorially coordinated heteroatoms are typical for Mn(III) complexes; the chain axis shows a distinct

Table VII. Selected Bond Distances (Å) and Angles (deg) for **5**

Mn–Na	3.297 (1)	Mn–O5	2.270 (6)
Mn–O1	1.898 (5)	Mn–N1	2.032 (6)
Mn–O2	1.911 (4)	Mn–N2	2.052 (6)
Mn–O3	2.120 (5)		
Na–O1	2.409 (5)	Na–O4	2.357 (6)
Na–O2	2.368 (4)		
Mn–O1–Na	99.2 (2)	Mn–O2–Na	100.3 (2)
O5–Mn–O3	174.5 (2)	O2–Mn–O1	86.9 (2)
O2–Na–O1	66.5 (2)	N2–Mn–N1	93.1 (2)
O1–Na–O4	81.5 (2)	O2–Na–O4	81.1 (2)
C22–O8	1.44	O8–O8'	2.232 (66)
H22–O8	1.116 (33)		
	H22–O8–C22	119.9 (4)	

Table VIII

complex no.	μ_{eff},[a] μ_B	J, cm^{-1}	IR bands, cm^{-1}
1	4.85	−1.72	1617, 1543, 1468, 1444, 1396, 1306
2	5.02	0[b]	2065, 1613, 1547, 1468, 1448, 1338, 1303, 809
3	4.76 [6.73]	ND[c]	1623, 1540, 1531, 1466, 1448, 1338, 1303
4	4.85 [6.86]	−3.55	1627, 1530, 1455, 1423, 1378, 1298
5	5.01 [7.08]	0	1616, 1572, 1546, 1472, 1446, 1407, 1298

[a] Numbers in brackets are per complex. [b] Zero by necessity for a mononuclear complex. [c] Not determined.

elongation of the Mn–O bond (Mn–O1 = 1.876 (4) Å) vs the average Mn–O(acetate) length, which is consistent with a Jahn–Teller distortion of this high-spin d^4 ion.

Mn(2-OH-SALPN)NCS. The reaction that produced **1** can also yield a mononuclear complex with the addition of an excess of a monodentate ligand, in this case thiocyanate. The green thiocyanate complex **2** was characterized by its infrared spectrum and a range of physicochemical parameters (Table VIII). This complex is five-coordinate with N-bonded thiocyanate occupying an axial position. A manganese–nitrogen bond, in preference to a manganese–sulfur bond, is supported by ν_{C-N} at 2065 cm^{-1} and ν_{C-S} at 809 cm^{-1}, which have previously been associated with metal–nitrogen coordination.[17] Furthermore, a discrete mononuclear complex, rather than a thiocyanate chain as observed for Mn(ACAC)$_2$NCS (ACAC = acetylacetonate), is also supported by the IR data. Most important to this assignment is the shift of ν_{C-N} to 2080 cm^{-1} in the ACAC chain. The solid-state magnetic susceptibility (μ_{eff} = 5.0 μ_B) also demonstrates the mononuclear nature of the manganese centers in this complex.

[Mn$_2$(2-OH-SALPN)$_2$(CH$_3$OH)]·CH$_3$OH. Cationic, mononuclear complexes are formed when **1** or **2** is dissolved in methanol. Addition of 1 equiv of NaOH or NaOMe facilitates the conversion of these monomeric compounds into the dimeric form **3**. The details of this conversion are described in the following paper. Various physicochemical studies indicated that **3** was a dimetallic complex. These included the depressed magnetic moment for the manganese(III) metal centers and the generation of 2 equiv of Mn(2-OH-SALPN)$^+$ cation with added acid.

Two types of dimers have previously been reported for tetradentate manganese Schiff base complexes, as shown in Figure 3. Both bis(μ-oxo) and bis(μ-hydroxo) linkages have been proposed for [Mn^{IV}(SALPN)O]$_2$[9] and [Mn^{III}(SALPN)(OH)]$_2$,[18] respectively. A brief structural report of what is most likely the Mn(IV)/Mn(IV) dimer has appeared.[18] An alternative structure is a bis(μ-phenolato) bridge. Examples of this geometrical arrangement include the weakly associated Mn(SALEN)Cl (SALEN = dianion of N,N'-disalicylideneethylenediamine),[19] the Mn(II) dimer [Mn(SALPS)]$_2$ [SALPS = dianion of N,N'-[1,1'-dithiobis(phenylene)]bis(salicylideneamine)][20] and the
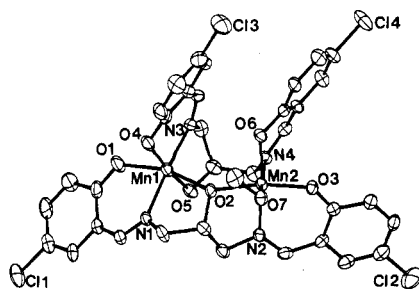
(17) Stults, B. R.; Marianelli, R. S.; Day, V. W. *Inorg. Chem.* **1975**, *14*, 722.
(18) Masleu, H. S.; Waters, T. N. *J. Chem. Soc., Chem. Commun.* **1973**, 760.
(19) Pecoraro, V. L.; Butler, W. M. *Acta Crystallogr.* **1986**, *C42*, 1151.
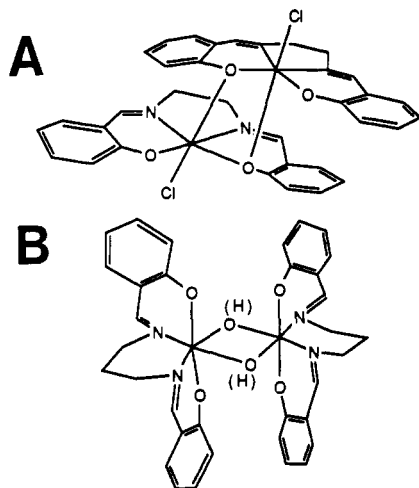
Figure 3. Two previously observed dinuclear structures of manganese-(III) Schiff base complexes: (A) bis(μ-phenolato) bridges; (B) bis(μ-oxo) or bis(μ-hydroxo) bridges.


Figure 4. ORTEP diagram of Mn₂(2-OH-(5-Cl-SAL)PN)₂(CH₃OH) (4) (showing atom-numbering scheme) with thermal ellipsoids of 50% probability.

Mn(III) dimer [Mn(bpy)₂(Sal)]₂ (Sal = salicylate).[18]

None of these structural motifs appeared appropriate for the dimer **3**. The formation of a bis(phenolato) bridge should be independent of added hydroxide or methoxide ion. The infrared spectra of **3** when synthesized with Na¹⁸OH, NaOCH₃, and NaOH were identical. This spoke strongly against either oxo or hydroxo bridges linking the Mn(III) ions. Even sodium acetate, when used in excess, quantitatively generated **3** from **2**.

We have observed that X-ray-quality crystals of manganese Schiff base complexes can often be obtained from the analogous halide ring-substituted material. To this end, the ligand 2-OH-(5-Cl-SAL)PN was used to obtain X-ray-quality crystals of the 5-chloro derivative **4** by slow evaporation of a methanol solution. The data in Table VIII confirm that **4** is the desired ring-substituted relative of **3**.

This unique dimer is illustrated as Figure 4. Important bond lengths and angles for **4** are provided in Table VI. An alkoxide oxygen (O2) is the only directly bridging atom between centers. As a result, the manganese(III) ions exhibit the largest separation yet observed for an alkoxide-, oxide- or phenolate-bridged manganese dimer (3.80 Å, Table VI). Each trianionic ligand distributes five heteroatoms between the two metals. The first 2-OH-(5-Cl-SAL)PN group acts as a symmetrical binucleating ligand with imino phenolate atoms O1 and N1 coordinated to Mn1 and the two atoms O3 and N2 coordinated to Mn2. The alkoxide oxygen (O2) acts as an unsymmetric bridge between the two metals (Mn1–O2 = 2.32 Å; Mn2–O2 = 1.90 Å). The second ligand is best considered as a tridentate chelating agent about Mn1, with atoms O4, N3, and O5, which is tethered by an ethylene bridge to a bidentate chelating agent, with atoms N4 and O6, that encapsulates Mn2. The sixth position of the Mn2 coordination
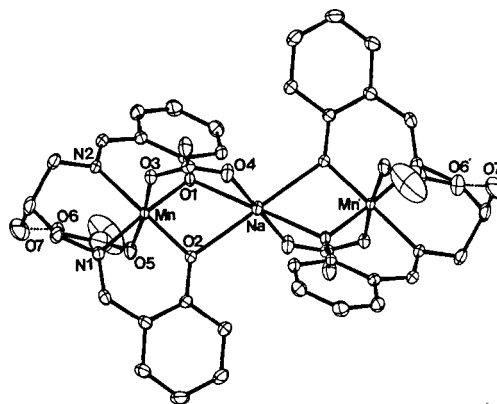
Figure 5. ORTEP diagram of the anionic portion of [C₂H₉O₂][NaMn₂-(2-OH-SALPN)₂(OAc)₄]·2H₂O (5) (showing the atom-numbering scheme) with the terminal ellipsoids of 50% probability. This structure illustrates the hydrogen bonding between oxygen atoms O6 and O7 in the intramolecular configuration.

sphere is filled by a methanol (O7) molecule.

Both manganese ions show severely distorted octahedral structures, as expected for high-spin Mn(III). Elongation along the O1–Mn1–O2 axis is very pronounced. For example, a comparison of Mn1–O1 (2.08 Å) and Mn1–O4 (1.89 Å) or Mn1–O2 (2.32 Å) and Mn1–O5 (1.88 Å) demonstrates a >0.2-Å lengthening of the metal–heteroatom distances. Because of the weakened Mn1–O2 bond, the Mn2–O2 interaction is strong (1.90 Å). The Jahn–Teller distortion for Mn2 occurs along the N4–Mn2–O7 axis. Once again, this is illustrated by comparison of equivalent heteroatom–manganese bonds (Mn2–N2 = 1.99 Å and Mn2–N4 = 2.29 Å).

We and others[22-24] have shown the tridentate alkoxy imino phenolate ligands with five- and six-membered chelate rings form exclusively meridional isomers with manganese. This preference is the reason for the dramatically different ligand binding modes seen in **4**. The symmetrical ligand forms two adjacent meridional units by using the alkoxide, O2, as the hinge between two corner-shared, tetragonally distorted octahedra. This geometry has been observed often in binuclear copper complexes of 2-OH-SALPN[25] and, very recently, in a low-valent manganese cubane.[26] The second ligand cannot adopt a symmetrical orientation, which would lead to an edge-shared structure with a shorter manganese separation, and retain the meridional coordination preference since phenolate oxygen atoms O1 and O4 and atoms O3 and O6 would be required to occupy the same sites in the two manganese polyhedra. Therefore, the second unit of the ligand forms a meridonal tridentate chelate with Mn1 using O4, N3, and O5. The flexibility of the ethylene linkage then allows N4 and O6 to act as a bidentate imino phenolate donor to Mn2.

The Mn1 polyhedron is similar to that described for Mn(SA-LADHP)₂ [SALADHP = dianion of 2-methyl-2-(salicylidene-amino)-1,3-dihydroxypropane].[23] The primary differences are that Mn1 is in the +3 oxidation state, which leads to a Jahn–Teller distortion along the axis O1–Mn1–O2, while a more symmetric polyhedron is observed for the Mn(IV) atom in Mn(SALADHP)₂. In addition, the alkoxide oxygen, O2, in **4** forms a strong bond to Mn2 and a weak bond with Mn1 (2.317 Å), whereas very short Mn^{IV}–O alkoxide distances (average 1.87 Å) are seen in the monomer. As discussed in the following paper, these structural differences have a profound effect on the manganese redox couples.

(20) Kessissoglou, D. P.; Butler, W. M.; Pecoraro, V. L. *Inorg. Chem.* **1987**, 26, 495.

(21) Vincent, J. B.; Folting, K.; Huffman, J. C.; Christou, G. *Inorg. Chem.* **1986**, 25, 996.

(22) Kessissoglou, D. P.; Butler, W. M.; Pecoraro, V. L. *J. Chem. Soc., Chem. Commun.* **1986**, 1253.

(23) Kessissoglou, D. P.; Li, X.; Butler, W. M.; Pecoraro, V. L. *Inorg. Chem.* **1987**, 26, 2787.

(24) Mikuriya, M.; Torihara, N.; Okawa, H.; Nida, S. *Bull. Chem. Soc. Jpn.* **1987**, 54, 1063.

(25) Mazurek, W.; Kennedy, B. J.; Murray, N. S.; O'Connor, M. J.; Rogers, J. R.; Snow, M. R.; Wedd, A. G.; Zurach, P. R. *Inorg. Chem.* **1985**, 24, 3258.

(26) Brooker, S.; McKee, V.; Shepard, W. B.; Pannell, L. K. *J. Chem. Soc., Dalton Trans.* **1987**, 2555.
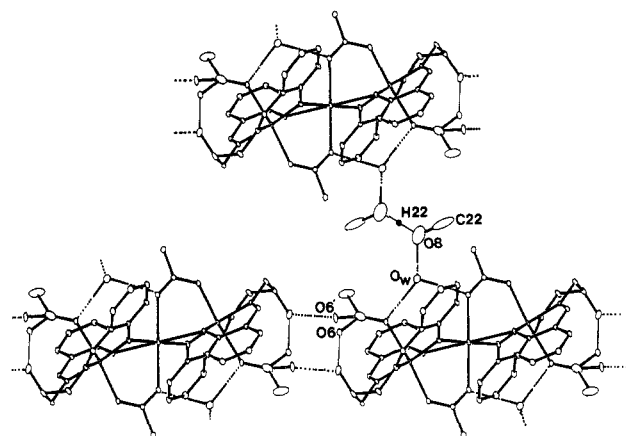
Figure 6. Hydrogen-bonding network in a crystal of **5**. The disorder of monodentate acetates (O6 and O6') and the two primary models for charge balance are described in the text.
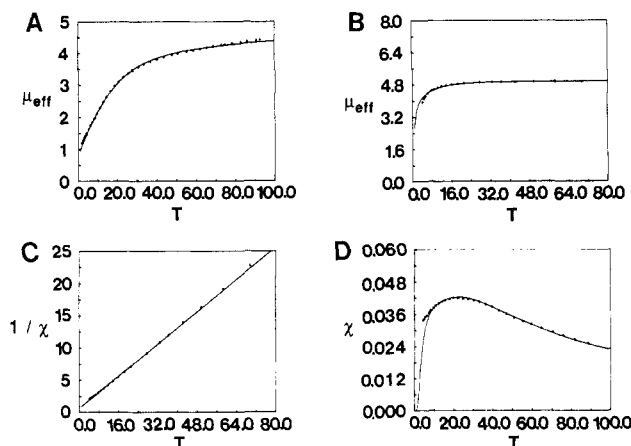

Figure 7. Variable-temperature magnetic susceptibility plots for (A) complex **1**, (B, C) complex **5**, and (D) complex **4**.

Previously described, singly bridging alkoxo[24] or phenolato[19] manganese dimers and trinuclear complexes[27,28] have in every case been stabilized by acetate moieties spanning the two metals. Copper complexes of 2-OH-SALPN show the ligand acting as a pentadentate chelating agent with the μ-alkoxo bridge.[29] A greater diversity of stabilizing bridging ligands (e.g., pyrazolate) are reported in the copper systems. Yet, the dimeric structural type seen with **4** has not been observed even in these analogously Jahn–Teller-distorted d^9–d^9 compounds.

$[C_2H_9O_2][NaMn_2(2\text{-OH-SALPN})_2(OAc)_4]\cdot2H_2O$. Green, triclinic crystals suitable for X-ray studies are isolated if 1 equiv of sodium methoxide is reacted with **1** in methanol. An ORTEP diagram of the anion in this material, $[C_2H_9O_2][NaMn_2(2\text{-OH-}SALPN)_2(OAc)_4]\cdot2H_2O$ (**5**), is illustrated in Figure 5. A modified packing diagram showing the $[C_2H_9O_2]^+$ cation and the disorder in the coordinated acetates is given in Figure 6. Selected bond lengths and angles are provided in Table VII.

The anion, $[NaMn_2(2\text{-OH-SALPN})_2(OAc)_4]^-$, is composed of two $Mn^{III}(2\text{-OH-SALPN})$ units that are linked through a completely encapsulated Na^+ ion which is located on a crystallographic inversion center. The sodium ion cage is formed by two phenolate bridges, O1 and O2, from each Mn(2-OH-SALPN) moiety and by two acetates that also bridge the manganese and sodium ions. The sodium octahedron is markedly distorted. This is best shown by the O1–Na–O2 angle of 66.5° and the O1–Na–O2' angle of 113.5°. In contrast, the Na–O distances are very similar, ranging from 2.36 to 2.41 Å. The manganese(III) ions are also six-coordinate; however, the distortion from octahedral geometry for this metal is through a tetragonal elongation along the Mn–O-(acetate) bonds. Asymmetric Mn–O(acetate) bonds are apparent with the oxygen atom of the bridging acetate, O3, at a relatively short 2.12 Å while O5 of the monodentate acetate is at a very long distance, 2.27 Å. The Mn(III) to 2-OH-SALPN heteroatom distances (Table VII) are very similar to those observed in the chain (Table V).

The significant disorder of the monodentate acetate moieties is illustrated in Figure 6. A strong intramolecular hydrogen bond to the pendant hydroxyl (O7) is illustrated by the thin line connecting O6 and O7 in Figure 6. Alternatively, a strong intermolecular hydrogen bond (dotted lines) is formed when O6' interacts with the hydroxyl proton of an adjacent anion, O7'.

The hydrogen bond network in the crystal has importance beyond the simple description of the disorder in the monodentate acetates. The $[C_2H_9O_2]^+$ cation, with proton H22 on a crystallographic inversion center, is illustrated in Figure 6. The

O8–O8' distance is very short (2.23 Å) and is reminiscent of the oxygen–oxygen separation seen in the $H_3O_2^-$ anion (2.27 Å).[30] Thus, there is a very strong, symmetrical interaction between H22 and the methanol oxygen atoms. Our preferred hydrogen-bonding network is illustrated in Figure 6 by assigning solid lines for O–H bonds and dotted lines for O–H hydrogen bonds. The $[C_2H_9O_2]^+$ ion forms a hydrogen bond to the water molecule O_w, which in turn forms hydrogen bonds to metal-bound oxygens of the bridging and monodentate acetates of the anion. With use of this formalism, each acetate is an anion and each 2-OH-SALPN is a dianion. Thus, these ligands contribute a charge of 8– to this unit cell. The two Mn(III) and the Na(I) contribute a charge of 7+. Neutrality is achieved with the $C_2H_9O_2^+$ cation. An alternative description treats the methanol-derived ion as the $C_2H_7O_2^-$ anion. In this model, the solid lines connecting O8 and O_w and O_w and O5 are O–H hydrogen bonds and the dotted lines are O–H bonds. A structure with two neutral, coordinated acetic acid groups, two anionic bridging acetates, and two dianionic 2-OH-SALPN ligands giving a total charge of 6– results. The metal cation charge remains unchanged at 7+. Charge balance is achieved by using the $C_2H_7O_2^-$ anion. The latter model explains the very short O8–O8' distance (2.23 Å) and the very long Mn–O5 distance (2.27 Å). However, we prefer the first description, as this requires a simple cationic species neutralizing a complex anion. The second model places in close proximity a strong base, $C_2H_7O_2^-$, and a reasonable acid, a metal-bound acetic acid moiety. Because we cannot locate the protons in this structure, further discussion is unwarranted; however, some combination of these two extremes is probably operable.

Considerable attention has been focused on the tendency of metallo Schiff base complexes to form higher nuclearity clusters through bridging mono- and divalent cations.[31] Trinuclear species in both cis[32] [e.g., $[Na(THF)_2(CoSALEN)_2]^+$] and trans[33] [e.g., $Na(THF)_2(CoSALEN)_2$] configurations have been structurally characterized. Complex **5**, as required by the crystallographic inversion center, is of the latter category. The tetragonal planes of the two manganese ions are parallel, leading to a chair conformation for the six-atom grouping Mn–O1–O2'–Mn'–O1'–O2. The sodium ion sits in the center of this array. cis-[Na-$(THF)_2(CoSALEN)_2]^+$ [32] and trans-$Na(THF)_2(CoSALEN)_2$[33] are structures in which four of the six coordination sites of the Na^+ are provided by bridging ligands. Similarly, cis-Na-$(ClO_4)(NiACEN)_2$ [ACEN = dianion of N,N'-bis(acetylacetonyl)ethylenediamine][34] substitutes bidentate perchlorate ion

(27) Li, X.; Kessissoglou, D. P.; Kirk, M. L.; Bender, C. A.; Pecoraro, V. L. *Inorg. Chem.* **1988**, *27*, 1.
(28) Kessissoglou, D. P.; Kirk, M. L.; Bender, C. A.; Lah, M. S.; Pecoraro, V. L. *J. Chem. Soc., Chem. Commun.* **1989**, 84.
(29) (a) Nishida, Y.; Kida, S. *Inorg. Chem.* **1988**, *27*, 447. (b) Borer, L. L.; Sinn, E. *Inorg. Chim. Acta* **1988**, *142*, 197.

(30) Abdu-Dari, K.; Raymond, K. N.; Freyberg, D. P. *J. Am. Chem. Soc.* **1979**, *101*, 3688.
(31) Sinn, E.; Harris, L. M. *Coord. Chem. Rev.* **1969**, *4*, 391.
(32) Randaccio, L. *Gazz. Chim. Ital.* **1974**, *104*, 991.
(33) Arena, F.; Floriani, C.; Zanazzi, P. F. *J. Chem. Soc., Chem. Commun.* **1987**, 183.
(34) Armstrong, L. G.; Lip, H. C.; Lindoy, L. F.; McPartlin, M.; Tasker, P. A. *J. Chem. Soc., Dalton Trans.* **1977**, 1771.

for the monodentate THF molecules. A remarkable pentanuclear complex[35] formed by the condensation of diphenylketene (dpk) with Co(SALEN), {(CoSALEN)$_2$Na$_2$[CoSALEN(dpk)$_2$]}·3THF, contains completely encapsulated sodium ions with four- and five-coordination. However, to our knowledge, the cage structure in **5** provides the first example of complete encapsulation of an alkali-metal cation by bridging ligands in a discrete trinuclear formulation.

Magnetic Behavior of Complexes 1, 4, and 5. The complexes **1**, **4**, and **5** provide a structural series with remarkable diversity of bridging interactions. Spin exchange between manganese(III) centers can occur through axially bridging acetates as in **1**, through a combination of acetates and phenolates as in **5**, or through an alkoxide bridge as in **4**.

Exchange interactions between Mn(III) centers in compound **1** are mediated through a single acetate bridge. The temperature dependence of the magnetic moment is shown in Figure 7A, and the data are consistent with antiferromagnetic interactions. Heisenberg exchange theory was utilized to analyze the data, where the Hamiltonian

$$H = -2J \sum_{i=1}^{N-1} S_i \cdot S_{i+1} \tag{1}$$

was employed. The solid line is the best fit to the data, where

$$\mu_{eff} = 2.828[\chi_{mol}T]^{1/2} \tag{2}$$

and the molar magnetic susceptibility per ion is given by the polynomial expression[36]

$$\chi_{chain} = (Ng^2\mu_\beta^2)(kT)^{-1}[(A(s) + [B(s)]x^2) \times (1 + [C(s)]x + [D(s)]x^3)^{-1}] \tag{3}$$

For the case of the $S = 2$ linear chain, $A = 2.000$, $B = 71.938$, $C = 10.428$, $D = 955.56$, and $x = J/kT$. The low-temperature data (<10 K) could not be described by eq 3 due to chain-end effects, caused by grinding the sample prior to packing into the sample holder. In this case, the chain ends would be expected to obey the Curie law and eq 3 was modified to take this into account:[37]

$$\chi_{obsd} = [PNg^2\mu_\beta^2 S(S + 1)(3kT)^{-1} + (100 - P)\chi] \tag{4}$$

where $S = 2$, g is that of the chain, and P is the percentage of ions obeying the Curie law. Although it is impossible to distinguish between chain-end effects and monomeric impurities, low-temperature SQUID measurements on uncrushed crystals of compound **1** show no Curie tail.[38] A good fit ($R = 0.90\%$) was obtained from the best fit of eq 4 to the data and yielded the parameters $J = -1.72$ cm^{-1}, $g = 1.97$, and $P = 2.49\%$. This is very similar to the published values for the analogous Mn(SALEN)OAc chain ($g = 1.98$, $J = -1.5$ cm^{-1}).[39] However, in contrast to the case for Mn(SALEN)OAc, interchain interactions appear to be negligible. Since the g value for the Mn(III) ion in a D_{4h} environment should equal 2, the low value for g obtained from the fit may be a result of the highly distorted environment about manganese in this compound or the effects of zero-field splitting (vide infra).

Complex **5** provides another variant on an acetate-bridged structure. Floriani has described[33] a mixed-valence Na-(THF)$_2$Co$^{II/I}$(SALEN)$_2$ cluster with crystallographically equivalent Co(SALEN) units. Therefore, this complex has either a completely delocalized ground state or a rapid, reversible electron-transfer process between the two cobalt ions. This suggests that the sodium ion can mediate this electron transfer or ground-state delocalization. In contrast, the magnetic behavior

of Cu(II)–Mg(II)–Cu(II) Schiff-base compounds display Curie–Weiss behavior with small values for the Weiss constant.[32] Figure 7B shows that compound **5** obeys the Curie–Weiss law with $g = 2.07$ and $\Theta = -2.08$ K. The absence of a maximum in the susceptibility of this compound to 2 K implies that magnetic exchange interactions are small if present at all. However, the severe moment reduction at low temperatures warrants some consideration.

The ground state of high-spin Mn(III) in a tetragonal environment is an orbital singlet, and the spin degeneracy is partially removed by spin–orbit coupling. The magnetic properties of such a system can be described by the spin Hamiltonian (5), which

$$\mathcal{H} = g_\parallel \beta H_z \cdot S_i + g_\perp \beta(H_x \cdot S_x + H_y \cdot S_y) + D[S_z^2 - \tfrac{1}{3}S(S + 1)] \tag{5}$$

consists of both Zeeman and zero-field splitting components.[40] A rhombic term has not been included since it has very little effect on the magnetic susceptibility unless it is significantly large. In light of the crystal structure, the idealized D_{4h} symmetry was utilized in the analysis of the data for simplicity. The spin Hamiltonian operates on the spin eigenfunctions within the $|2\rangle$, $|1\rangle$, $|0\rangle$, $|-1\rangle$, $|-2\rangle$ basis, and diagonalization of the matrix elements yields five eigenvalues. The eigenvalues were substituted into eq 6, the thermodynamic expression for the susceptibility. The derivatives with respect to the field, $\partial E/\partial B$, were calculated by the

$$\chi_{\cos\phi} = -N/B[(\sum_i \partial E_i/\partial B[\exp(-E_i/kT)])/\sum_i \exp(-E_i/kT)] \tag{6}$$

use of the Hellman–Feynman theorem. A spatial averaging technique, making use of the Labatto quadrature[41] in the numerical integration of (7), was used to calculate the powder average molar magnetic susceptibility.[42]

$$\chi_{av} = \tfrac{1}{2}\int_0^\pi \chi_{\cos\phi} \sin\phi \, d\phi \tag{7}$$

The temperature variation of the magnetic moment may be fit to eq 7, and the solid line in Figure 7C corresponds to the best fit parameters $g_\parallel = 2.00$, $g_\perp = 2.05$, and $D = -6.13$ cm^{-1}. The R factor for the fit was 1.5%. The structural evidence for axial elongation, coupled with the large negative value for the zero-field splitting parameter, provides strong evidence supporting a $^5B_{1g}$ ground state with the d$_{z^2}$ orbital being the highest occupied orbital.

Compound **4** is dimeric, and the superexchange pathway is through a single alkoxide bridge (vide supra). The individual Z axes in this molecule are oriented at an approximately 130° angle, and superexchange proceeds formally from the d$_{z^2}$ orbital of Mn1 to the d$_{x^2-y^2}$ orbital of Mn2. Since the d$_{x^2-y^2}$ orbital is unoccupied when D is negative, magnetic exchange interactions would be negligible for the d$_{z^2}$–d$_{x^2-y^2}$ pathway. Such a situation is actually observed in the linear chain Na$_2$[Mn$^{III}_2$(Sal)$_4$(CH$_3$OH)$_2$].[43] Of course, since the metal environment is considerably distorted from the idealized D_{4h} geometry, mixing of d$_{z^2}$ and d$_{x^2-y^2}$ is likely. This provides a plausible exchange mechanism promoting weak antiferromagnetic exchange.

In view of the low symmetry about both ions in the dimer and the crystallographic inequivalence of the two centers, the spin-Hamiltonian approach was not used due to overparameterization. The Hamiltonian (8) was used instead in the analysis of the data.

$$\mathcal{H} = -2JS_1 \cdot S_2 \tag{8}$$

The magnetic susceptibility per ion of a pair of exchange-coupled $S = 2$ ions is given by (9), where $x = J/kT$. The solid line in Figure 7D was constructed from the best fit of eq 9 to the experimental data, which assumes a symmetrical model, where the

(35) Arena, F.; Floriani, C.; Chiesi-Villa, A.; Guastini, C. *Inorg. Chem.* **1986**, *25*, 4589.
(36) Hiller, W.; Strahle, J.; Datz, A.; Hanack, M.; Hatfield, W. E.; ter Haar, L. W.; Gutlich, P. *J. Am. Chem. Soc.* **1984**, *106*, 329.
(37) Ginsberg, A. P. *Inorg. Chim. Acta* **1971**, *5*, 45.
(38) Renard, J.-P. Private communication.
(39) Kennedy, B. J.; Murray, K. S. *Inorg. Chem.* **1985**, *24*, 1552.

(40) Carrington, A.; McLachlan, A. D. *Introduction to Magnetic Resonance*; Harper and Row: New York, 1967.
(41) Scarborough, J. P. *Numerical Mathematical Analysis*; Oxford University Press: New York, 1971; p 159.
(42) Marathe, V. R.; Mitra, S. *Chem. Phys. Lett.* **1974**, *27*, 103.
(43) Pecoraro, V. L.; Kessissoglou, D. P. Unpublished observation.

$$\frac{Ng^2\mu_\beta^2}{2kT} =$$

$$\frac{60 + 28\exp(-4x) + 10\exp(-7x) + 2\exp(-9x)}{9 + 7\exp(-4x) + 5\exp(-7x) + 3\exp(-9x) + \exp(-10x)} \tag{9}$$

best fit parameters are $J = -3.55$ cm^{-1} and $g = 1.95$ with an R value of 0.8%. The deviation of the fit at low temperature (<10 K) is a result of the asymmetry of the dimer. The relatively low g value is a good indication of this structural asymmetry and large zero-field splitting.

Conclusion

Manganese(III) Schiff base complexes provide a rich series of structural types that can be used as models for the magnetic and structural properties of manganoenzymes. The propensity of manganese to form carboxylate-bridged clusters suggests that amino acids such as aspartate and glutamate may provide structural integrity to biological manganese clusters. The Mn$^{III}_2$Mn^{II}(SALADHP)$_2$(OAc)$_4$(CH$_3$OH)$_2$ complexes in both linear[28] and bent[29] geometries clearly document this tendency. The isolation of **5** extends the range of structures in this family to mixed manganese–alkali-metal cation complexes. Alkaline-earth ions also promote the formation of loosely associated clusters.[44] This observation, taken together with biophysical studies of higher plant photosynthesis, may provide insight toward the structure of the manganese cluster(s) involved in biological water oxidation. A strict calcium requirement is observed for both oxygen-evolving activity and production of the S$_2$ state multiline signal of the thylakoid membrane associated oxygen-evolving complex (OEC) of photosystem II.[45,46] It is also known that

sodium competes for at the least one of the calcium binding sites in the OEC.[47] The D1 and D2 peptides, which most likely contain the manganese ions, are rich in carboxylate residues.[48] Thus, it is quite possible that the calcium functions to provide stability to the manganese cluster in higher oxidation states.[46] This stability may be imparted through stabilization of the protein structure by a direct association with the cluster via carboxylate bridges as observed for concanavalin A.[49] Complex **5** provides an example of how such a redox-inactive metal could promote manganese cluster formation.

(44) Fenton, D. E.; Bresciani-Pahor, N.; Calligaris, M.; Nardin, G.; Ranadaccio, L. *J. Chem. Soc., Dalton Trans.* **1979,** 39.
(45) Carumarata, K.; Cheniae, G. M. *Plant Physiol.* **1987,** *84,* 587.

(46) Ghanotakis, D. F.; Topper, J. N.; Babcock, G. T.; Yocum, C. F. *FEBS Lett.* **1984,** *170,* 169.
(47) Waggoner, C.; Pecoraro, V. L.; Yocum, C. F. *FEBS Lett.* **1989,** *244,* 237.
(48) Trebst, Z. *Z. Naturforsch.* **1986,** *41C,* 240.
(49) Hardman, K. D.; Ainsworth, C. F. *Biochemistry* **1972,** *11,* 4910.

Contribution from the Departments of Chemistry, The University of Michigan, Ann Arbor, Michigan 48109, and University of Massachusetts, Amherst, Massachusetts 01003

Structurally Diverse Manganese(III) Schiff Base Complexes: Solution Speciation via Paramagnetic ¹H NMR Spectroscopy and Electrochemistry

Joseph A. Bonadies,[1] Michael J. Maroney,*[2] and Vincent L. Pecoraro*[1,3]

The mononuclear cation Mn(2-OH-SALPN)$^+$ (2-OH-SALPN = dianion of *N,N'*-disalicylidene-2-hydroxypropanediamine) converts cleanly to a novel monoalkoxy-bridged dimer, Mn$^{III}_2$(2-OH-SALPN)$_2$(solvent), by the stoichiometric addition of sodium methoxide or tetrabutylammonium hydroxide in methanol, DMF, or acetonitrile. This conversion, which involves deprotonation of the ligand alcohol group, can be followed by using cyclic voltammetry and ¹H NMR spectroscopy. The monomer undergoes reduction [Mn(III/II)] at −182 mV vs SCE in methanol. The Mn(III) dimer has metal-based oxidations at +230 and +1600 mV. Comparison of these redox processes with those of the structurally related mononuclear Mn(IV) complex Mn(SALADHP)$_2$ [SALADHP = dianion of 2-methyl-2-(salicylideneamino)-1,3-dihydroxypropane] indicates that the Mn(IV) oxidation state has been destabilized by nearly 700 mV in the dimer by the presence of a bridging alkoxide ligand. Both the monomer and dimer give rise to isotropically shifted ligand proton NMR resonances due to the presence of paramagnetic high-spin Mn(III) centers. With use of ring-substituted derivatives, the hyperfine shifted resonances have been assigned to specific ligand protons. The ¹H NMR spectrum obtained for the monomer consists of relatively sharp peaks assigned to phenolate protons at −21.9 (5'-H) and −23.8 (4'-H) ppm and a broad resonance at +28.1 ppm that is assigned to the proton on the 2-carbon atom of the propane backbone. The resonance due to this last proton is absent from the spectrum of the dimer, which exhibits phenolate proton resonances at −3.4 (6'-H), −5.3 (4'-H), and −13.7 (5'-H) ppm. This information has allowed characterization of species in solution, including a trinuclear complex, [NaMn$^{III}_2$(2-OH-SALPN)$_2$(OAc)$_4$]$^-$, which forms both the monomeric cation and dimer in solution.

Introduction

It is now recognized that manganese plays an important role in numerous redox processes associated with the metabolism of

dioxygen. This has prompted recent attempts to understand the coordination chemistry of Mn(III) ions, which are now believed to play a role in at least three enzymes: manganese superoxide dismutase (MnSOD),[4] manganese catalase,[5] and the photosyn-

(1) The University of Michigan.
(2) The University of Massachusetts.
(3) G. D. Searle Biomedical Research Scholar (1986–1989), Alfred P. Sloan Fellow (1989–1991).

(4) Recent reviews that discuss these points are: Pecoraro, V. L. *Photochem. Photobiol.* **1988,** *48,* 249. Babcock, G. T. Photochemistry. In *New Comprehensive Biochemistry*; Amesz, J., Ed.; Elsevier: Amsterdam, 1987; Vol. 15, p 125.